ACS OMEGA

http://pubs.acs.org/journal/acsodf

Article

Fluorescent Polypropylene Nanoplastics for Studying Uptake, Biodistribution, and Excretion in Zebrafish Embryos

Wang Sik Lee, Hyunjung Kim, Yugyeong Sim, Taejoon Kang, and Jinyoung Jeong*

Cite This: *ACS Omega* 2022, 7, 2467−2473

Read Online

ACCESS | Metrics & More | Article Recommendations | Supporting Information

ABSTRACT: Nanoplastics (NPs) are emerging environmental pollutants and are a significant concern for human health. The small size of NPs allows them to accumulate within and adversely affect various tissues by penetrating the gastrointestinal barrier. However, most toxicity studies on NPs have been based on commercial polystyrene nanoparticles. Among plastics, polypropylene (PP) is one of the most widely used, and it is continuously micronized in the environment. Although PP has high potential for forming NPs by weathering, little is known about the biological effects of polypropylene nanoplastics (PPNPs) due to a lack of particle models. Here, we present a simple and high-yield method for PPNP production by nonsolvent-induced phase separation. The synthesized PPNPs were spherical in shape, with an average diameter of 562.15 ± 118.47 nm and a high yield of over 84%. These PPNPs were fluorescently labeled by the combined swelling-diffusion method to study their biodistribution after exposure to developing zebrafish embryos (ZFEs). We found that the fluorescent PPNPs were internalized by ingestion, distributed in the intestine of developing ZFEs, and eventually excreted. This study will aid evaluations of the potential risks of environmentally relevant plastics at the nanoscale.

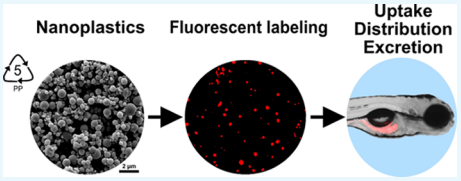

1. INTRODUCTION

Nanoplastics (NPs), defined as small plastic debris with sizes on the nanometer scale (1−1000 nm), are an emerging concern due to the potential risks that they pose to the environment and public health.[1,2] Due to their physicochemical properties, nanosized materials can interact with biological systems and induce deleterious effects.[3,4] This fact implies that NPs may have adverse effects on living organisms. To date, many studies have reported the adverse effects of NPs, such as oxidative stress and inflammatory reactions, in diverse organisms, including plankton, zebrafish, and mice, under experimental conditions.[5,6] In particular, NPs are known to penetrate human tissues by crossing the lung, skin, and gastrointestinal barriers and can cause side effects in the human body.[7] Thus, attention should be given to the risk posed by NPs. However, most of the risk assessments of NPs involve polystyrene (PS) as a particle model because it is commercially available with various sizes and surface charges.[7] Although PS is a widely used plastic type, polyethylene and polypropylene (PP) constitute a large portion of the plastic debris detected in the environment, but studies on these NPs are limited.[8,9] In particular, PP is the most widely used plastic, with applications ranging from food packaging to automotive parts, and is also a significant component of personal protective equipment such as masks, the use of which has increased due to the COVID-19 pandemic.[10−13] A considerable amount of PP waste has accumulated in the environment and is continuously converted to PP microplastics by external factors such as UV radiation, oxidation, and biofilms.[14] PP microplastics have been detected in the gastrointestinal tracts of sea turtles on the Atlantic coastline of Florida at 96 h posthatching.[15] Additionally, a recent study reported that PP microplastics were released from infant bottles during formula preparation.[16] In a study using human-derived cell and animal models (zebrafish and nematodes), PP microplastics were shown to induce cytotoxicity, proinflammatory cytokine production, oxidative stress, and intestinal damage.[17,18] Fragmentation of PP accumulated in the environment does not stop at the micro level but continues until nanosized particles are formed. Thus, further studies are needed to understand the potential effects of polypropylene nanoplastics (PPNPs). Likewise, a recent study suggested that preparation and labeling techniques of PPNPs as model plastic nanomaterials are important for improving toxicological and biodistribution studies.[19]

In this study, we developed a facile method to prepare PPNPs as model NPs to study the biological effects of nanoscale PP in an animal model. A recent study suggested that the preparation of PPNPs as model plastic nanomaterials and a subsequent labeling technique were important to improve toxicological and biodistribution studies. PPNPs were produced with high yield (>84%) by nonsolvent-induced phase separation (NIPS), which is a unique method that is neither a bottom-up method, such as polymerization, nor a top-down method, such as ball milling or cryomilling.[20,21] The

Received: December 1, 2021
Accepted: December 23, 2021
Published: January 4, 2022

https://doi.org/10.1021/acsomega.1c06779
ACS Omega 2022, 7, 2467−2473

physical and chemical properties of the as-prepared PPNPs were fully characterized using scanning electron microscopy (SEM), dynamic light scattering, Fourier-transform infrared (FT-IR) spectroscopy, and differential scanning calorimetry (DSC) and successfully fluorescently labeled for visualization of their biofate in zebrafish embryos (ZFEs) as an animal model.

2. RESULTS AND DISCUSSION

2.1. Preparation and Characterization of PPNPs. PPNPs were prepared by the NIPS method, which is a phase separation technique based on polymer solubility in a good solvent and a nonsolvent (Figure 1a).[22] We used xylene as a good solvent and ethanol as a nonsolvent, which induced phase separation and recrystallization of PP particles. For nanosized PP particles, key factors include the type of nonsolvent, PP concentration, and volumetric ratio of good solvent to nonsolvent. For example, water is a representative nonsolvent for NIPS, and it is not suitable for use in our method due to its immiscibility with xylene.[23] As seen in Figure S1, porous particles were formed by using water as a nonsolvent for PPNP preparation. The powerful advantages of this method are its simplicity and high production yield (over 84%, Table S1) compared to those of common methods to produce NPs and microplastics, such as ball-milling methods, which require complicated equipment, are time consuming, and have low NP yields.

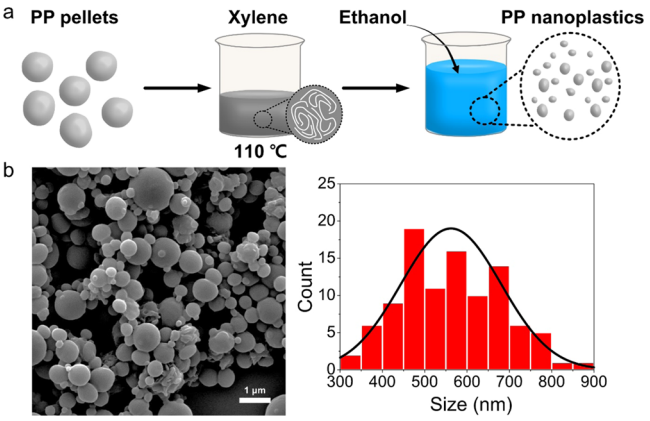

Figure 1. (a) Scheme for preparation of the polypropylene nanoplastics (PPNPs) using a modified nonsolvent-induced phase separation (NIPS) method. (b) SEM images and the size distribution (n = 100).

The morphological, chemical, and thermal properties of the as-synthesized PPNPs were analyzed. The field-emission scanning electron microscopy (FE-SEM) image shows that the PPNPs were sphere-like particles with a size of 562.15 ± 118.47 nm (Figure 1b). The chemical and thermal properties of the PPNPs were analyzed by FT-IR spectroscopy (Figure 2a) and DSC (Figure 2b), respectively. FT-IR spectroscopy is a simple and nondestructive chemical analysis technique that uses infrared light and is the most common analytical method for identifying polymers.[24] The FT-IR spectra of the PP pellets as a control and those of the PPNPs consistently showed peaks at 2950, 2915, and 2838 cm^{-1} attributed to C−H stretching; a peak at 1455 cm^{-1} attributed to CH_2 bending; a peak at 1377 cm^{-1} attributed to CH_3; and peaks at 1166, 997, 840, and 808 cm^{-1} attributed to C−H and C−C bonds (Figure 2a).[24] The FT-IR analysis indicated that no chemical change occurred between the PP pellets and PPNPs. DSC is a technique for analyzing the response of polymers to heating and identifies polymers based on their melting point (M_p), glass transition temperature, and crystallization temperature (T_c).[25] Figure 2b shows the DSC thermogram of the PP pellets and PPNPs, and the detailed melting results are summarized in Table S2. In the DSC thermogram, the double crystal melting peak of the PP pellets and PPNPs was observed at approximately 140∼160 °C, representing the α-crystal form, which is a relatively large crystal with a high melting temperature ($T_{m\text{-}high}$), and the β-crystal form, which is a small crystal with a low melting temperature ($T_{m\text{-}low}$).[26] Interestingly, the $T_{m\text{-}low}$ of the PPNPs was slightly higher (149.54 °C) than that of the PP pellets (147.53 °C), and the proportion of the β-crystal form in the PPNPs was higher than that in the PP pellets, as seen in the inset of Figure 2b. This finding indicated that the PPNPs consisted mainly of small crystals, whereas the PP pellets consisted of a slightly higher proportion of α-crystals than of β-crystals. Moreover, the T_c values differed, with a value of 115.40 °C for the PP pellets and 120.87 °C for the PPNPs, consistent with the higher $T_{m\text{-}low}$ of the PPNPs.[26] However, the M_p ($T_{m\text{-}high}$) and crystallinity (X_{DSC}) were not different between the PPNPs and PP pellets (Table S2). Overall, DSC analysis suggested that the PPNPs were slightly reconstructed to a relatively small crystal form (i.e., β-crystal) during synthesis, but there was no significant change in the thermal properties.

2.2. Fluorescence Labeling of PPNPs. Fluorescence labeling is a general strategy for monitoring and visualizing

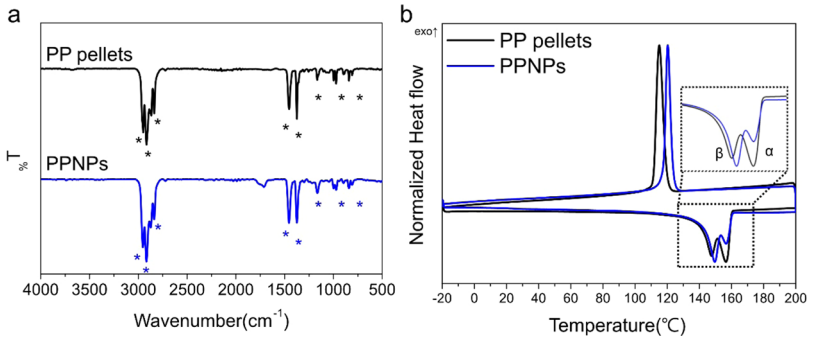

Figure 2. (a) FT-IR spectra of PP pellets and PPNPs (ATR mode, scan range 500∼4000 cm^{-1}). (b) DSC thermogram (second cycle, range −20 °C ∼ 200 °C).

https://doi.org/10.1021/acsomega.1c06779
ACS Omega 2022, 7, 2467−2473

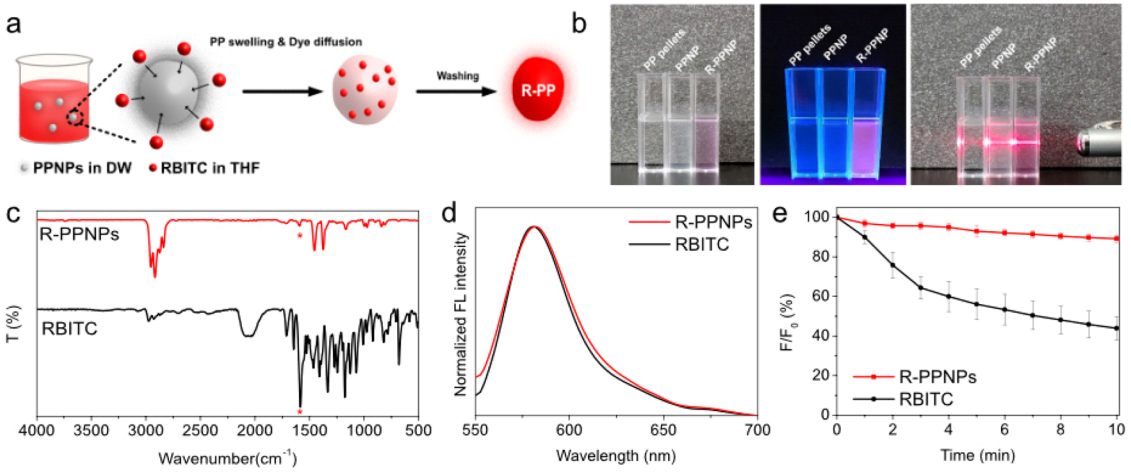

Figure 3. (a) Scheme of fluorescence labeling of PPNPs by the CSD method. (b) Photographs of PP pellets, PPNPs, and R-PPNP suspension in DW under visible light (left), UV light (365 nm, middle), and visible light with laser beam (right). (c) FT-IR spectra, (d) fluorescence spectra, and (e) fluorescence stability of RBITC and R-PPNPs.

NPs.[27−30] The combined swelling-diffusion (CSD) method is a common approach to prepare fluorescent NPs and involves the entrapment of fluorescent molecules inside a polymer matrix by controlling the temperature or solubility.[31,32] In this work, we chose solubility-based CSD to fluorescently label PPNPs, using tetrahydrofuran (THF) as a good solvent and distilled water (DW) as a poor solvent. When THF swells the PPNPs, rhodamine B isothiocyanate (RBITC) diffuses into the swollen PPNPs. Simultaneously, DW maintains the spherical shape of the NPs to minimize the surface area and provides an environment in which RBITC can diffuse into the PP via THF (Figure 3a). After separation, red fluorescent PPNPs (RBITC-labeled PPNPs, R-PPNPs) were obtained. The photographic image on the left in Figure 3b clearly shows opaque PPNPs and pink R-PPNPs compared to the transparent PP pellets. In addition, compared to the nonfluorescent PP pellet and PPNPs, the R-PPNPs exhibited bright fluorescence under UV irradiation. Moreover, the colloidal dispersibility was clearly indicated based on the observable laser beam path in both PPNP and R-PPNP solutions due to the Tyndall scattering effect (the image on the right in Figure 3b).

Morphology and chemical structure are closely related to biological effects such as distribution, clearance, and toxicity.[33,34] Thus, we confirmed the morphological and chemical properties of the R-PPNPs. The R-PPNPs were 567.3 ± 107.6 nm in size, with a spherical shape similar to that of PPNPs (Figure S2). The FT-IR spectrum of the R-PPNPs was also similar to that of the PPNPs, except for a peak at 1581 cm^{-1}, attributed to RBITC (red asterisk) (Figure 3c). This result indicated that fluorescence labeling did not influence the chemical structure and that RBITC was successfully entrapped in the PPNPs. The fluorescence of the R-PPNPs was similar to that of RBITC, exhibiting emission at 580 nm upon excitation at 540 nm (Figure 3d). Moreover, the amount of RBITC entering the PPNPs was measured using a standard curve (Figure S3). The coefficient of determination (R^2) from the standard curve was 0.9886, and the amount of RBITC was 0.28 μg in 5 μg of R-PPNP. Finally, the fluorescence stability of the R-PPNPs dispersed in DW was evaluated over time by measuring the change in fluorescence intensity to confirm RBITC entrapment. As shown in Figure 3e, the fluorescence intensity of RBITC decreased by 56% after 10 min of exposure, while that of the R-PPNPs was maintained at 89% of the initial intensity. This result revealed that RBITC was successfully entrapped inside the PPNPs to prevent photobleaching. Therefore, photostable fluorescent PPNPs were prepared by the CSD method without morphological or chemical changes and were suitable for biomonitoring, such as for analysis of the uptake and fate of PPNPs in biological entities.

Water solubility is an important factor for bioassays of plastic particles, which are generally not dispersible in aqueous media, such as water, due to their hydrophobicity. Interestingly, the as-synthesized PPNPs were highly dispersible in an aqueous solution, even after fluorescence labeling. We assumed that the sonication process might influence the surface tension or surface energy of the spherical and heterogeneous PPNPs, resulting in good dispersibility of the PPNPs. Consequently, physicochemical characteristics such as the hydrodynamic size and zeta potential value of the PPNPs were evaluated. The hydrodynamic size of the PPNPs in DW was 1095 ± 39.18 nm (Figure S4a), and the zeta potential value was −58.53 ± 1.76 mV (Figure S4b), indicating that the PPNPs were partially agglomerated in DW. We further measured the hydrodynamic size and zeta potential value in E3 egg water (EW), which is the culture medium used for ZFEs. The hydrodynamic size in EW increased to 1422 ± 70.15 nm, and the zeta potential decreased to −46.33 ± 1.17 mV, indicating that the agglomeration and the decrease in the surface charge of PPNPs might be caused by the electrolytes (e.g., NaCl; $CaCl_2$) present in EW.[35]

2.3. Uptake, Distribution, and Excretion of R-PPNPs in ZFEs. ZFEs are a representative animal model used for the risk assessment of NPs due to the high fecundity, rapid embryonic development, and embryo transparency of these organisms.[36] Several studies have demonstrated the uptake and fate of NPs with fluorescently labeled polystyrene nanoplastics (PSNPs) using ZFEs.[37−40] In a similar manner, we used ZFEs as an animal model to study the uptake and distribution of PPNPs. To minimize external blockage, ZFEs were dechorionated and treated with R-PPNPs before (24 hpf) and after (72 hpf) mouth opening of ZFEs. After 24 h of exposure to R-PPNPs at each timepoint, the mortality and deformity of the ZFEs were measured. Table S3 shows that the mortality and deformity of the ZFE-exposed R-PPNPs were not significantly

https://doi.org/10.1021/acsomega.1c06779
ACS Omega 2022, 7, 2467−2473

different from those of the control at either 48 or 96 hpf. Moreover, we evaluated the mortality and deformity of PPNPs without fluorescence labeling. The mortality and deformity of the PPNP-exposed ZFEs were similar to those of R-PPNP-treated ZFEs. This result indicates that fluorescence labeling marginally affected the toxicity of PPNPs.

To observe the uptake and biodistribution of R-PPNPs in ZFEs, R-PPNPs were treated before and after zebrafish mouth opening at 24 and 72 hpf, respectively. In Figure 4, differential

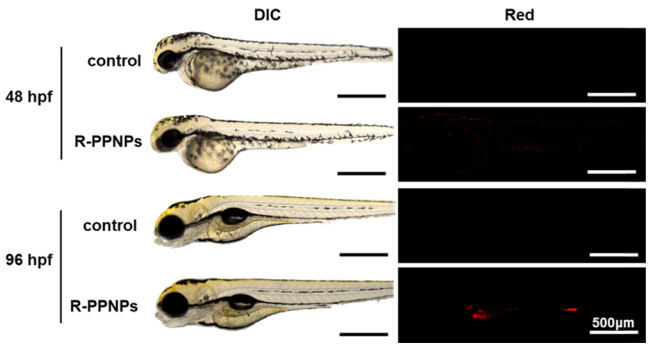

Figure 4. Optical and fluorescence images of zebrafish embryos with or without R-PPNP treatments at 24 and 72 hpf. These images were taken after 24 h exposure.

interference contrast (DIC) and red fluorescence images show the control and R-PPNP-treated ZFEs at different time points of 48 and 96 hpf, representing 24 h of exposure. Interestingly, weak fluorescence was detected along the skin of R-PPNP-treated ZFEs at 48 hpf, while red fluorescence was clearly seen in the gastrointestinal tract of R-PPNP-treated ZFEs at 96 hpf (Figure 4). This result revealed that the R-PPNPs, which were approximately 567 nm in diameter, did not penetrate the skin of the ZFEs but could be ingested via the mouth and localized in the gastrointestinal tract. We further confirmed the biodistribution of the R-PPNPs both before and after mouth opening by cross-sectional image analysis of ZFEs. Figure S5 shows that there was no red fluorescence in any region of a large portion of the yolk sac in ZFEs at 48 hpf after 24 h of treatment with R-PPNPs, similar to the results for the control zebrafish (Figure S6). However, the cross-sectional images of the intestinal bulb and mid-intestine of the ZFEs after 24 h of treatment with R-PPNPs at 72 hpf clearly showed red fluorescent dots in the intestinal lumen (*lu*), which is the internal space of the intestine (Figure 5a). Apparently, the R-PPNPs were close to the intestinal epithelium (*e*) in the (*i*) region in Figure 5a but did not penetrate the epithelium, indicating that the R-PPNPs were taken up by the ZFEs via ingestion and translocated into the intestine but not absorbed for digestion. In addition, we further observed R-PPNP uptake in the ZFEs up to 124 hpf and found that the ingested R-PPNPs were excreted by peristalsis, which is a wave-like movement associated with intestinal function. In Figure 5b, the time-lapse fluorescence images of zebrafish larvae after R-PPNP ingestion show that the fluorescent dots (white arrow) moved toward the anal passages and were ultimately excreted from the body over a period of 40 min. For quantitative analysis of the excreted R-PPNPs from the ZFEs, we measured the amount of R-PPNPs remaining in the ZFEs after exposure at 96 and 120 hpf by measuring the fluorescence intensity. The amount of R-PPNPs at 96 hpf was approximately 1.01 ± 0.09 μg/individual and decreased to 0.46 ± 0.10 μg/individual after 24 h of depuration, indicating that approximately 45% of the R-PPNPs were excreted from the ZFEs (Figure S6). In a previous study, the half-life of elimination of PSNPs (24 and 250 nm) in scallops was shown to be approximately 1.4 days, which was quite similar to our result despite the different plastic types and sizes.[41] Overall, it was clearly demonstrated that the R-PPNPs were useful model materials for the uptake, distribution, and excretion study of PPNPs in animal models such as ZFEs.

3. CONCLUSIONS

The health impact of NPs is an important issue to consider when predicting the potential risk of plastic fragmentation in environments. Although NPs are known to be widespread and accumulate in environments, it is difficult to assess the

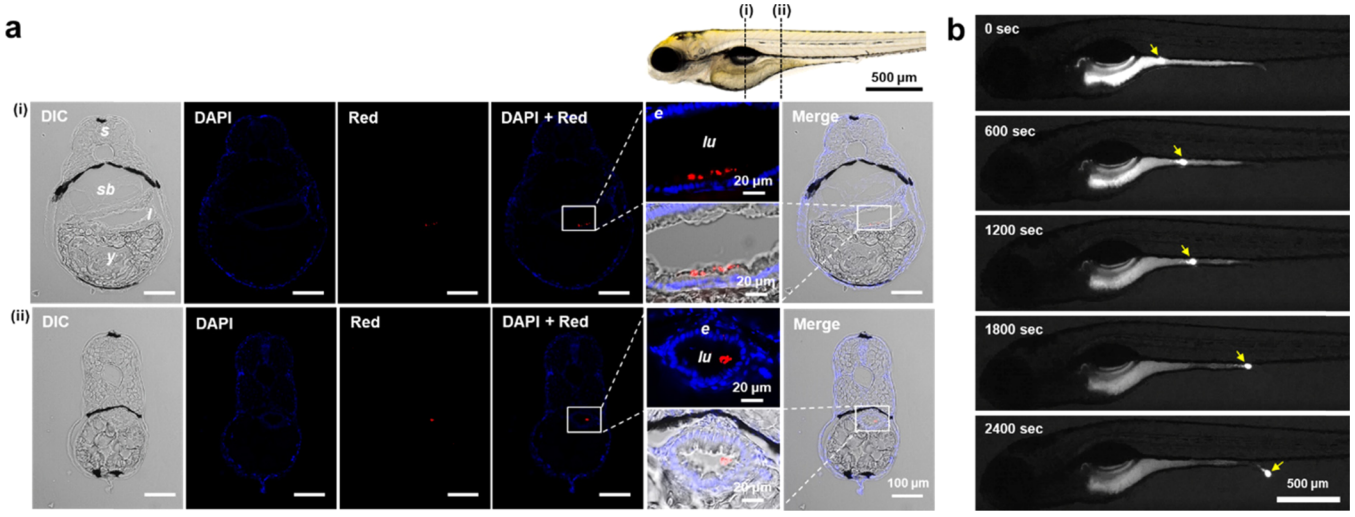

Figure 5. (a) Cross-sectional images of ZFEs at 96 hpf after R-PPNP exposure at 72 hpf for 24 h at the region of (i) intestinal bulb and (ii) mid-intestine with three different filters, such as DIC, DAPI, and red. (b) Time-lapse fluorescence photograph of ZFEs at 124 hpf after R-PPNP exposure at 72 hpf for 24 h. The yellow arrow indicates the agglomeration of R-PPNPs. Abbreviations: *S*, somite; *SB*, swim bladder; *I*, intestine; *lu*, intestinal lumen; *e*, intestinal epithelium; and *Y*, yolk.

https://doi.org/10.1021/acsomega.1c06779
ACS Omega 2022, 7, 2467−2473

potential risks of these materials due to limitations of detection and monitoring and the lack of model NPs. In particular, although PP is widely used in packaging and personal protective equipment such as masks, gloves, and clothes and although the consumption and wastage of these products have increased due to the COVID-19 pandemic, it is hard to monitor PPNPs in the environment or investigate their biological impact in vitro and in vivo without model particles. In this study, we demonstrated the preparation of PPNPs, examined their physical and chemical properties as model NPs, and performed fluorescence labeling to monitor the biological behavior of PPNPs in zebrafish as an animal model. This study provides a simple, high-yield preparation method for PPNPs by the NIPS method. Furthermore, plastic particles were successfully fluorescently labeled by the CSD method to observe PPNP behavior in ZFEs as an animal model. This is an exceptional study on NPs other than PS, which is a major plastic type in NP research. Thus, these PPNPs could be practically used as model NPs for further studies, such as for monitoring, detection, and biological effect analysis.

4. EXPERIMENTAL SECTION

4.1. Materials and Reagents. PP pellets, xylene, THF, and RBITC were purchased from Sigma-Aldrich. Ethyl alcohol (anhydrous, 99.9%) was purchased from Samchun Chemicals (Seoul, Korea). Polytetrafluoroethylene (PTFE, 0.2 μm pore size, 47 mm, Omnipore hydrophilic membrane filter) and polyvinylidene fluoride (PVDF, 0.2 μm pore size, 47 mm, Durapore hydrophilic membrane filter) were purchased from Millipore, USA. To observe the biodistribution and excretion using ZFEs, pronase (P8811) and tricaine (ethyl 3-aminobenzoate methanesulfonate salt) were purchased from Sigma-Aldrich. EW was prepared by dissolving 5 mM NaCl, 0.17 mM KCl, 0.33 mM $CaCl_2$, and 0.33 mM $MgSO_4$ in 1 L of DW according to previous work.[40]

4.2. Preparation of PPNPs. PP pellets (0.13 g) were added to xylene (20 mL) and heated to 110 °C for 30 min with vigorous stirring. When PP was completely dissolved in xylene, heating was stopped, and ethanol (100 mL) as a nonsolvent was simultaneously added to the PP solution. The solution was stirred for 3 h until it had cooled enough. Then, the precipitated products were collected by vacuum filtration using a 0.2 μm PTFE membrane filter and dried at 80 °C overnight.

4.3. Characterization of PPNPs. Morphological properties were measured by FE-SEM (Quanta 250 FEG, FEI). PPNP suspension in ethanol was dropped and dried on the silicon wafer. After drying, the gold ion was coated for 60 s using a sputter coater (Polaron SC7640, Quorum Technologies, Ltd.) for FE-SEM measurement. The size distribution of the PPNPs from the FE-SEM image was evaluated using ImageJ software. The physicochemical properties were analyzed with a particle size analyzer (Zetasizer Nano ZS, Malvern Instruments) after resuspension of PPNPs in DW by sonication for 10 min using a bath-type sonicator (DH.WUC. A03H, Daihan Scientific, Korea). Polymer identification of PPNP powder was performed using FT-IR spectroscopy (Alpha-T, Bruker) and DSC (DSC 1, Mettler-Toledo). DSC was performed from −20 to 200 °C at a heating rate of 5 °C min^{-1}, and the polymer crystallinity was calculated based on the DSC thermogram using the following equation:[42]

$$X_{DSC} = (\Delta H_m/\Delta H_m^*) \times 100\% \quad (1)$$

where ΔH_m is the melting enthalpy of PP measured by DSC, and $\Delta H_m^*$is 207.1 J/g, which is the melting enthalpy of 100% crystalline PP.

4.4. Fluorescence Labeling of PPNPs. PPNPs were fluorescently labeled by the CSD method for biodistribution analysis.[31] Twenty milligrams of PPNPs was added to 9 mL of DW and sonicated for 10 min. Three milliliters of an RBITC solution (1 mg mL^{-1}) in THF was added to the PPNP solution followed by stirring for 3 days. After stirring, the R-PPNPs were separated by vacuum filtration using a 0.2 μm PVDF filter to remove unlabeled RBITC in the reaction solution and dried at room temperature. The morphology and chemical structure of the R-PPNPs were analyzed by FE-SEM and FT-IR spectroscopy, respectively. Fluorescence spectra were measured using a fluorescence spectrometer (FS-2, SINCO, South Korea). Photostability was evaluated by comparing changes in the fluorescence intensity using a multimode microplate reader (Cytation5, BioTek Inc., USA) with excitation/emission wavelengths of 540/580 nm for 10 min at 1 min intervals.

4.5. Zebrafish Maintenance. Zebrafish AB strains were maintained at 28.5 °C with a light cycle of 14 h light/10 h dark and fed brine shrimp twice per day. The ZFEs were obtained by using the following process. Male and female zebrafish were set up as pairs before mating in breeding tanks with a divider. The divider was removed the next morning, and the zebrafish were stimulated with light. The eggs were dropped on the bottom of the tank and collected, pooled, and rinsed with EW. Prior to the experiments, fertilized eggs were observed under a stereomicroscope (S6D, Leica, UK), and dead/unfertilized embryos were removed.

4.6. In Vivo Experiments of R-PPNPs on ZFEs. Healthy ZFEs at 24 h postfertilization (hpf) were treated with pronase (1 mg mL^{-1}) to remove the chorion. Prior to exposure, R-PPNPs were added to EW and sonicated for 10 min until resuspended. Then, the dechorionated embryos were placed in a 6-well culture plate containing 50 ppm R-PPNPs in 5 mL of solution per well at 24 and 72 hpf. The R-PPNP-treated ZFEs were rinsed with fresh EW after 24 h of incubation, anesthetized with tricaine, and observed under an upright clinical microscope (Eclipse Ci, Nikon) with fluorescence filters (DAPI filter set, excitation/emission at 375/460 nm, mCherry filter set, excitation/emission at 570/645 nm) under halogen lamp illumination at 48 and 96 hpf. Transverse sections of ZFEs were prepared by fixing with 4% paraformaldehyde at 4 °C, embedding in an agar block, soaking in a 30% sucrose solution, and cryosectioning to a thickness of 25 μm. Fluorescence images of the sectioned ZFEs were obtained by upright microscopy with a fluorescence filter and monochrome camera (Progres Gryphax@Rigel, Jenoptik, Germany). All zebrafish experiments were performed in compliance with the guidelines of the Korea Research Institute of Bioscience and Biotechnology (KRIBB), and the experimental protocols were approved by KRIBB-IACUC (approval number: KRIBB-AEC-20283).

4.7. Mortality and Deformity of R-PPNP-Treated ZFEs. The acute toxicity of R-PPNPs is based on the assessment of mortality and deformity. Ten dechorionated embryos were exposed to EW containing 50 ppm R-PPNPs at 24 and 72 hpf. After incubation for 24 h, the endpoint was measured using a microscope (SMZ18, Nikon, Japan). The rate of mortality was (dead embryos)/(10 embryos) × 100. The deformity of ZFEs includes morphological defects such as pericardial edema, yolk

https://doi.org/10.1021/acsomega.1c06779
ACS Omega 2022, 7, 2467−2473

edema, yolk necrosis, curved tails, fin deformities, and head malformation. The rate of deformity was (abnormal embryos)/(10 embryos) × 100. All experiments were performed in triplicate.

4.8. Statistical Analysis. Statistical tests were performed by one-way analysis of variance using Origin 2020b software (Origin Lab Corporation Inc., USA). Tukey's test was used to compare the toxic effects of the PPNPs and R-PPNPs against controls. A significant difference was observed when $p < 0.05$.

■ ASSOCIATED CONTENT

Supporting Information

The Supporting Information is available free of charge at https://pubs.acs.org/doi/10.1021/acsomega.1c06779.

The yield of PPNPs by the NIPS method (Table S1), DSC melting results of PP pellets and PPNPs (Table S2), mortality and deformity of PPNP- and R-PPNP-treated ZFEs (Table S3), SEM images of PPNPs using DW as a nonsolvent (Figure S1), SEM images and size distribution of R-PPNPs (Figure S2), standard curve for the fluorescence intensity of RBITC (Figure S3), hydrodynamic size and zeta potential measurements of PPNPs (Figure S4), cross-sectional images of ZFEs at 48 hpf after R-PPNP exposure at 24 hpf for 24 h (Figure S5), cross-sectional images of control ZFEs at 48 and 96 hpf (Figure S6), and the standard curve of R-PPNPs and the comparison of R-PPNPs in ZFE at 96 and 120 hpf after exposure at 72 hpf for 24 h (Figure S7) (PDF)

■ AUTHOR INFORMATION

Corresponding Author

Jinyoung Jeong − *Environmental Disease Research Center, Korea Research Institute of Bioscience and Biotechnology (KRIBB), Daejeon 34141, Republic of Korea; Department of Nanobiotechnology, KRIBB School of Biotechnology, University of Science and Technology (UST), Daejeon 34113, Republic of Korea;* orcid.org/0000-0003-0381-3958; Email: jyjeong@kribb.re.kr

Authors

Wang Sik Lee − *Environmental Disease Research Center, Korea Research Institute of Bioscience and Biotechnology (KRIBB), Daejeon 34141, Republic of Korea*

Hyunjung Kim − *Environmental Disease Research Center, Korea Research Institute of Bioscience and Biotechnology (KRIBB), Daejeon 34141, Republic of Korea*

Yugyeong Sim − *Environmental Disease Research Center, Korea Research Institute of Bioscience and Biotechnology (KRIBB), Daejeon 34141, Republic of Korea; Department of Nanobiotechnology, KRIBB School of Biotechnology, University of Science and Technology (UST), Daejeon 34113, Republic of Korea*

Taejoon Kang − *Bionanotechnology Research Center, Korea Research Institute of Bioscience and Biotechnology (KRIBB), Daejeon 34141, Republic of Korea;* orcid.org/0000-0002-5387-6458

Complete contact information is available at: https://pubs.acs.org/10.1021/acsomega.1c06779

Author Contributions

W.S.L. and H.K. designed and performed the synthesis, characterization, and fluorescence labeling of polypropylene nanoplastics. Y.S. performed the zebrafish experiment and analysis on the sample via microscopic observation. J.J. conceived the idea and supervised the project. T.K. provided the analytical feedback. W.S.L and J.J. mainly wrote the manuscript, and all authors read, provided the feedback, and approved the final manuscript.

Notes

The authors declare no competing financial interest.

■ ACKNOWLEDGMENTS

This work was supported by the Basic Science Research Program (NRF-2019R1C1C1006084) and the Brain Research Program (NRF-2019M3C7A1031534) and Center for BioNano Health Guard as Global Frontier Project (HUGARD_2013M3A6B2078950) through the National Research Foundation of Korea (NRF) funded by the Ministry of Science and ICT of Korea (MSIT), the National Research Council of Science & Technology (NST) grant by the Korea government (MSIT) (No.CAP-20022-000), and the KRIBB Research Initiative Program (KGM5322113 and KGS1282113).

■ ABBREVIATIONS

NPs, nanoplastics; PP, polypropylene; PPNPs, polypropylene nanoplastics; NIPS, nonsolvent-induced phase separation; CSD, combined swelling-diffusion; ZFEs, zebrafish embryos; PS, polystyrene; PE, polyethylene; SEM, scanning electron microscopy; DLS, dynamic light scattering; FT-IR, Fourier-transform infrared; DSC, differential scanning calorimetry; PTFE, polytetrafluoroethylene; PVDF, polyvinylidene fluoride; THF, tetrahydrofuran; RBITC, rhodamine B isothiocyanate; R-PPNPs, RBITC-labeled PPNPs; DW, distilled water; EW, E3 egg water; M_p, melting point; T_c, crystallization temperature; $T_{m\text{-}high}$, high melting temperature; $T_{m\text{-}low}$, low melting temperature; hpf, hours post fertilization; DIC, differential interference contrast

■ REFERENCES

(1) Hartmann, N. B.; Hüffer, T.; Thompson, R. C.; Hassellöv, M.; Verschoor, A.; Daugaard, A. E.; Rist, S.; Karlsson, T.; Brennholt, N.; Cole, M.; Herrling, M. P.; Hess, M. C.; Ivleva, N. P.; Lusher, A. L.; Wagner, M. Are We Speaking the Same Language? Recommendations for a Definition and Categorization Framework for Plastic Debris. *Environ. Sci. Technol.* **2019**, *53*, 1039−1047.

(2) Kihara, S.; Köper, I.; Mata, J. P.; McGillivray, D. J. Reviewing Nanoplastic Toxicology: It's an Interface Problem. *Adv. Colloid Interface Sci.* **2021**, *288*, No. 102337.

(3) Nel, A. E.; Mädler, L.; Velegol, D.; Xia, T.; Hoek, E. M. V.; Somasundaran, P.; Klaessig, F.; Castranova, V.; Thompson, M. Understanding Biophysicochemical Interactions at the Nano-Bio Interface. *Nat. Mater.* **2009**, *8*, 543−557.

(4) Mu, Q.; Jiang, G.; Chen, L.; Zhou, H.; Fourches, D.; Tropsha, A.; Yan, B. Chemical Basis of Interactions between Engineered Nanoparticles and Biological Systems. *Chem. Rev.* **2014**, *114*, 7740−7781.

(5) Peng, L.; Fu, D.; Qi, H.; Lan, C. Q.; Yu, H.; Ge, C. Micro- and Nano-Plastics in Marine Environment: Source, Distribution and Threats — A Review. *Sci. Total Environ.* **2020**, *698*, No. 134254.

(6) Yong, C. Q. Y.; Valiyaveettil, S.; Tang, B. L. Toxicity of Microplastics and Nanoplastics in Mammalian Systems. *Int. J. Environ. Res. Public Health* **2020**, *17*, 1509.

(7) Lehner, R.; Weder, C.; Petri-Fink, A.; Rothen-Rutishauser, B. Emergence of Nanoplastic in the Environment and Possible Impact on Human Health. *Environ. Sci. Technol.* **2019**, *53*, 1748−1765.

(8) de Ruijter, V. N.; Redondo-Hasselerharm, P. E.; Gouin, T.; Koelmans, A. A. Quality Criteria for Microplastic Effect Studies in the Context of Risk Assessment: A Critical Review. *Environ. Sci. Technol.* **2020**, *54*, 11692−11705.
(9) Koelmans, A. A.; Mohamed Nor, N. H.; Hermsen, E.; Kooi, M.; Mintenig, S. M.; De France, J. Microplastics in Freshwaters and Drinking Water: Critical Review and Assessment of Data Quality. *Water Res.* **2019**, *155*, 410−422.
(10) Aragaw, T. A. Surgical Face Masks as a Potential Source for Microplastic Pollution in the COVID-19 Scenario. *Mar. Pollut. Bull.* **2020**, *159*, No. 111517.
(11) Patrício Silva, A. L.; Prata, J. C.; Walker, T. R.; Duarte, A. C.; Ouyang, W.; Barcelò, D.; Rocha-Santos, T. Increased Plastic Pollution Due to COVID-19 Pandemic: Challenges and Recommendations. *Chem. Eng. J.* **2021**, *405*, No. 126683.
(12) Vanapalli, K. R.; Sharma, H. B.; Ranjan, V. P.; Samal, B.; Bhattacharya, J.; Dubey, B. K.; Goel, S. Challenges and Strategies for Effective Plastic Waste Management during and Post COVID-19 Pandemic. *Sci. Total Environ.* **2021**, *750*, No. 141514.
(13) Fadare, O. O.; Okoffo, E. D. Covid-19 Face Masks: A Potential Source of Microplastic Fibers in the Environment. *Sci. Total Environ.* **2020**, *737*, No. 140279.
(14) Min, K.; Cuiffi, J. D.; Mathers, R. T. Ranking Environmental Degradation Trends of Plastic Marine Debris Based on Physical Properties and Molecular Structure. *Nat. Commun.* **2020**, *11*, 727.
(15) White, E. M.; Clark, S.; Manire, C. A.; Crawford, B.; Wang, S.; Locklin, J.; Ritchie, B. W. Ingested Micronizing Plastic Particle Compositions and Size Distributions within Stranded Post-Hatchling Sea Turtles. *Environ. Sci. Technol.* **2018**, *52*, 10307−10316.
(16) Li, D.; Shi, Y.; Yang, L.; Xiao, L.; Kehoe, D. K.; Gun'Ko, Y. K.; Boland, J. J.; Wang, J. J. Microplastic Release from the Degradation of Polypropylene Feeding Bottles during Infant Formula Preparation. *Nat. Food* **2020**, *1*, 746−754.
(17) Hwang, J.; Choi, D.; Han, S.; Choi, J.; Hong, J. An Assessment of the Toxicity of Polypropylene Microplastics in Human Derived Cells. *Sci. Total Environ.* **2019**, *684*, 657−669.
(18) Lei, L.; Wu, S.; Lu, S.; Liu, M.; Song, Y.; Fu, Z.; Shi, H.; Raley-Susman, K. M.; He, D. Microplastic Particles Cause Intestinal Damage and Other Adverse Effects in Zebrafish Danio Rerio and Nematode Caenorhabditis Elegans. *Sci. Total Environ.* **2018**, *619-620*, 1−8.
(19) Cassano, D.; La Spina, R.; Ponti, J.; Bianchi, I.; Gilliland, D. Inorganic Species-Doped Polypropylene Nanoparticles for Multifunctional Detection. *ACS Appl. Nano Mater.* **2021**, *4*, 1551−1557.
(20) Paik, P.; Kar, K. K. Polypropylene Nanosphere: Particle Size and Crystal Structure. *Int. J. Plast. Technol.* **2009**, *13*, 68−82.
(21) Caldwell, J.; Lehner, R.; Balog, S.; Rhême, C.; Gao, X.; Septiadi, D.; Weder, C.; Petri-Fink, A.; Rothen-Rutishauser, B. Fluorescent Plastic Nanoparticles to Track Their Interaction and Fate in Physiological Environments. *Environ. Sci. Nano* **2021**, *8*, 502−513.
(22) Lu, W.; Yuan, Z.; Zhao, Y.; Zhang, H.; Zhang, H.; Li, X. Porous Membranes in Secondary Battery Technologies. *Chem. Soc. Rev.* **2017**, *46*, 2199−2236.
(23) Jung, J. T.; Kim, J. F.; Wang, H. H.; di Nicolo, E.; Drioli, E.; Lee, Y. M. Understanding the Non-Solvent Induced Phase Separation (NIPS) Effect during the Fabrication of Microporous PVDF Membranes via Thermally Induced Phase Separation (TIPS). *J. Membr. Sci.* **2016**, *514*, 250−263.
(24) Jung, M. R.; Horgen, F. D.; Orski, S. V.; Rodriguez, C. V.; Beers, K. L.; Balazs, G. H.; Jones, T. T.; Work, T. M.; Brignac, K. C.; Royer, S. J.; Hyrenbach, K. D.; Jensen, B. A.; Lynch, J. M. Validation of ATR FT-IR to Identify Polymers of Plastic Marine Debris, Including Those Ingested by Marine Organisms. *Mar. Pollut. Bull.* **2018**, *127*, 704−716.
(25) Drzeżdżon, J.; Jacewicz, D.; Sielicka, A.; Chmurzyński, L. Characterization of Polymers Based on Differential Scanning Calorimetry Based Techniques. *Trends Analyt. Chem.* **2019**, *110*, 51−56.
(26) Yu, K.; Jiang, H.; Zhou, H.; Mi, J.; He, Y.; Wang, X. Evolution of Double Crystal Melting Peak in Polypropylene Foam Assisted by β-Nucleating Agent and Supercritical CO2. *J. Appl. Polym. Sci.* **2018**, *135*, 1−10.
(27) Qu, M.; Li, D.; Qiu, Y.; Wang, D. Neuronal ERK MAPK Signaling in Response to Low-Dose Nanopolystyrene Exposure by Suppressing Insulin Peptide Expression in Caenorhabditis Elegans. *Sci. Total Environ.* **2020**, *724*, No. 138378.
(28) Chae, Y.; Kim, D.; Kim, S. W.; An, Y. J. Trophic Transfer and Individual Impact of Nano-Sized Polystyrene in a Four-Species Freshwater Food Chain. *Sci. Rep.* **2018**, *8*, 284.
(29) Della Torre, C.; Bergami, E.; Salvati, A.; Faleri, C.; Cirino, P.; Dawson, K. A.; Corsi, I. Accumulation and Embryotoxicity of Polystyrene Nanoparticles at Early Stage of Development of Sea Urchin Embryos Paracentrotus Lividus. *Environ. Sci. Technol.* **2014**, *48*, 12302−12311.
(30) Hwang, J.; Choi, D.; Han, S.; Jung, S. Y.; Choi, J.; Hong, J. Potential Toxicity of Polystyrene Microplastic Particles. *Sci. Rep.* **2020**, *10*, 7391.
(31) Lee, J. H.; Gomez, I. J.; Sitterle, V. B.; Meredith, J. C. Dye-Labeled Polystyrene Latex Microspheres Prepared via a Combined Swelling-Diffusion Technique. *J. Colloid Interface Sci.* **2011**, *363*, 137−144.
(32) Karakolis, E. G.; Nguyen, B.; You, J. B.; Rochman, C. M.; Sinton, D. Fluorescent Dyes for Visualizing Microplastic Particles and Fibers in Laboratory-Based Studies. *Environ. Sci. Technol. Lett.* **2019**, *6*, 334−340.
(33) Demir, E. A Review on Nanotoxicity and Nanogenotoxicity of Different Shapes of Nanomaterials. *J. Appl. Toxicol.* **2021**, *41*, 118−147.
(34) Braakhuis, H. M.; Park, M. V. D. Z.; Gosens, I.; de Jong, W. H.; Cassee, F. R. Physicochemical Characteristics of Nanomaterials That Affect Pulmonary Inflammation. *Part. Fibre Toxicol.* **2014**, *11*, 18.
(35) Peng, C.; Zhang, W.; Gao, H.; Li, Y.; Tong, X.; Li, K.; Zhu, X.; Wang, Y.; Chen, Y. Behavior and Potential Impacts of Metal-Based Engineered Nanoparticles in Aquatic Environments. *Nanomaterials* **2017**, *7*, 21.
(36) Lin, S.; Zhao, Y.; Nel, A. E.; Lin, S. Zebrafish: An in Vivo Model for Nano EHS Studies. *Small* **2013**, *9*, 1608−1618.
(37) Brun, N. R.; van Hage, P.; Hunting, E. R.; Haramis, A. P. G.; Vink, S. C.; Vijver, M. G.; Schaaf, M. J. M.; Tudorache, C. Polystyrene Nanoplastics Disrupt Glucose Metabolism and Cortisol Levels with a Possible Link to Behavioural Changes in Larval Zebrafish. *Commun. Biol.* **2019**, *2*, 382.
(38) Pitt, J. A.; Kozal, J. S.; Jayasundara, N.; Massarsky, A.; Trevisan, R.; Geitner, N.; Wiesner, M.; Levin, E. D.; Di Giulio, R. T. Uptake, Tissue Distribution, and Toxicity of Polystyrene Nanoparticles in Developing Zebrafish (Danio Rerio). *Aquat. Toxicol.* **2018**, *194*, 185−194.
(39) Pitt, J. A.; Trevisan, R.; Massarsky, A.; Kozal, J. S.; Levin, E. D.; Di Giulio, R. T. Maternal Transfer of Nanoplastics to Offspring in Zebrafish (Danio Rerio): A Case Study with Nanopolystyrene. *Sci. Total Environ.* **2018**, *643*, 324−334.
(40) Lee, W. S.; Cho, H. J.; Kim, E.; Huh, Y. H.; Kim, H. J.; Kim, B.; Kang, T.; Lee, J. S.; Jeong, J. Bioaccumulation of Polystyrene Nanoplastics and Their Effect on the Toxicity of Au Ions in Zebrafish Embryos. *Nanoscale* **2019**, *11*, 3173−3185.
(41) Al-Sid-Cheikh, M.; Rowland, S. J.; Stevenson, K.; Rouleau, C.; Henry, T. B.; Thompson, R. C. Uptake, Whole-Body Distribution, and Depuration of Nanoplastics by the Scallop Pecten Maximus at Environmentally Realistic Concentrations. *Environ. Sci. Technol.* **2018**, *52*, 14480−14486.
(42) Wang, S.; Zhang, J. Effect of Nucleating Agent on the Crystallization Behavior, Crystal Form and Solar Reflectance of Polypropylene. *Sol. Energy Mater. Sol. Cells* **2013**, *117*, 577−584.

https://doi.org/10.1021/acsomega.1c06779
ACS Omega 2022, 7, 2467−2473